LARGE-SCALE SEMI-EMPIRICAL PSEUDOPOTENTIAL ELECTRONIC STRUCTURE OF SELF-ASSEMBLED INGAAS QUANTUM DOTS

A THESIS SUBMITTED TO

THE GRADUATE SCHOOL OF ENGINEERING AND SCIENCE

OF BILKENT UNIVERSITY

IN PARTIAL FULFILLMENT OF THE REQUIREMENTS FOR

THE DEGREE OF

MASTER OF SCIENCE

IN

DEPARTMENT OF PHYSICS

By
Mustafa Kahraman
August 2018

LARGE-SCALE SEMI-EMPIRICAL PSEUDOPOTENTIAL ELEC-
TRONIC STRUCTURE OF SELF-ASSEMBLED InGaAs QUAN-
TUM DOTS
By Mustafa Kahraman
August 2018

We certify that we have read this thesis and that in our opinion it is fully adequate,
in scope and in quality, as a thesis for the degree of Master of Science.

———————————————
Ceyhun Bulutay(Advisor)

———————————————
Mehmet Özgür Oktel

———————————————
Cem Sevik

Approved for the Graduate School of Engineering and Science:

———————————————
Ezhan Karaşan
Director of the Graduate School

ABSTRACT

LARGE-SCALE SEMI-EMPIRICAL PSEUDOPOTENTIAL ELECTRONIC STRUCTURE OF SELF-ASSEMBLED INGAAS QUANTUM DOTS

Mustafa Kahraman
M.S. in Department of Physics
Advisor: Ceyhun Bulutay
August 2018

The so-called second quantum revolution emerged at the beginning of the second millennium, opening up a path to realization of spin-qubit-based quantum computing by means of controlling and protecting quantum coherent processes. Thus, along this spirit, the self-assembled quantum dots (SAQD) made a transition from conventional optoelectronic devices to spin-qubit applications. One specific problem that can benefit from this is the electron spin resonance (ESR) of a single-electron in a SAQD which could not be reproduced after its demonstration for more than ten years. The lack of insight for the electronic structure of SAQDs and g-factors changing with its properties might be the underlying reason for the decade-old puzzle. Towards the goal of understanding the ESR, atomistic large-scale semi-empirical electronic structures of InGaAs SAQDs having different shapes, sizes and indium concentrations are calculated using linear combination of bulk bands method. Two approaches to extract envelopes of the wave functions are demonstrated since the resulting wave functions have the fast fluctuations and understanding them might not be always possible. Calculated electronic structures and wave functions are compared and were found to be in agreement with the general theoretical and experimental findings paving the way to the calculation of g-factors in accordance with our eventual aim.

Keywords: InGaAs quantum dots, electronic structure, semi-empirical pseudopotential, linear combination of bulk bands .

ÖZET

INGAAS KUANTUM NOKTALARININ BUYUK OLCEKTE YARI-DENEYSEL POTANSIYELLERLE ELEKTRONIK YAPISI

Mustafa Kahraman
Fizik Bölümü, Yüksek Lisans
Tez Danışmanı: Ceyhun Bulutay
Ağustos 2018

İkinci binyılın başlangıcında ortaya çıkan ikinci kuantum devrimi, spin-kübit tabanlı kuantum bilgisayara bir yol açtı. Bu devrim ile beraber kendiliğinden bir araya gelmiş kuantum noktalar (KN) aygıt yapımı uygulamalarından ziyade spin-kübit uygulamalarında kullanılmak amacıyla araştırılmaya başlandı. Gösterildiği tarihten günümüze kadar, on yıllık süreçte bir KN'deki tek elektronun elektron spin rezonansı (ESR) tekrarlanamadı. Bunun en büyük nedeni KN'lerin elektronik yapılarının ve bu yapıların özellikleri ile değişen g-faktörünün teorik açıdan iyi anlaşılmadığından olabilir. ESR'nin tekrarlanamamasının nedenlerini anlama hedefine doğru, farklı şekil, boyut ve konsantrasyonlara sahip InGaAs (indiyum galyum arsenit) KN'lerin büyük ölçekli yarı-ampirik atomik elektronik yapıları, yığık bantların doğrusal bileşimi yöntemi kullanılarak hesaplanmıştır. Atomik yapının hesaplarda göz önünde bulundurulmasından kaynaklı, dalga fonksiyonlarının hızlı dalgalanmaktadır. Bundan ötürü dalga fonksiyonu zarflarını elde etmek için iki yöntem geliştirilmiştir. Değişik yapılarda InGaAs KN'leri için hesaplanmış elektronik yapılar ve dalga fonksiyonları karşılaştırılmış ve genel teorik ve deneysel bulgular ile uyumlu olduğu saptanmıştır. Bu da nihai hedefimiz olan g-faktörü hesapları için önemli bir aşama teşkil etmektedir.

Anahtar sözcükler: InGaAs kuantum noktalar, elektronik yapı, yarı-deneysel potansiyel, yığık, bantların doğrusal bileşimi.

iv

Acknowledgement

I cannot thank enough to my advisor Prof. Ceyhun Bulutay for his endless support and patience, but especially for his guidance which was not always necessarily for the academic matters. I am grateful and extremely lucky to get to know him and learn from him.

I would like express my gratitude to my thesis jury, Prof. Özgür Oktel and Assoc. Prof. Cem Sevik for kindly accepting to be in my jury and for their valuable time, comments and questions.

I thank to the faculty members and personal of the Physics Department, especially Prof. Cemal Yalabık whom I took most of my classes from in undergraduate and graduate studies. It feels impossible not to pursue knowledge after taking his classes.

It would have been very hard for me to write this thesis, if my colleague and more importantly friend Ekrem Taha Güldeste would not be there for me. I am more than grateful for his sincere friendship, support and valuable discussions. He is the man.

My second family also deserves an acknowledgment, Eren Çelik, Barış Evran and Dilara Yazıcı. Life would be very boring without them. They are irreplaceable.

I want to thank to my colleagues and friends in the faculty, Ahmed Ouf, Murod Bahovadinov, Yağmur Aksu Korkmaz and Oğuzhan Yörük for their valuable friendship and discussions. They were great help to me. People of the 14th Dormitory were also very kind, friendly and supportive in general. I would like to thank Ihsan, Fulya, Göksel, Theta Merve, Denizcan, Gamze and Nermin Abla. Dormitory life would be unbearable without them. Support and kindness of Nimet Abla will never be forgotten.

Lastly, without the endless support of my family, this thesis would not be

possible. I cannot thank enough to my mother Gülcan and my not so little brother Mete Han for their unlimited patience, support and kindness.

Contents

List of Figures

List of Tables

Chapter 1

Introduction

For the past few decades, semiconductor nanostructures has been attracting a great deal of interest which could be attributed to the rapidly developing, easily applicable growth techniques and to the range of possible novel device applications [2]. One of the most interesting quantum structures are self-assembled quantum dots (SAQDs) which confines the carriers in all spatial dimensions so that the energy spectrum becomes discrete. For this reason the cliche description is to call them as artificial atoms [3, 4].

The driving force behind the research on SAQDs used to be optoelectronic device applications, like semiconductor lasers [2]. Conventional lasers use quantum wells (QW) as the gain medium, but SAQDs were shown to be superior candidates to replace QWs as they exhibit better temperature stability, high differential gain efficiency and ultra-low threshold current density [5, 6, 7].

At the turn of the century there has been the so-called second quantum revolution which promoted quantum technologies as a stand-alone discipline [8]. Within this second quantum revolution, the flagship application is quantum computing which can be realized, among other alternatives, using QD spin qubits [9, 10, 11, 12]. For a recent account from a theoretician's perspective of the prospects of QD spin qubits in various solid-state realizations, see [13]. As the

electronic structure of QDs can be widely tuned by external magnetic, electric as well as electromagnetic fields [14], this makes them ideal playgrounds for the emerging arena of quantum simulators [15]. For spin-qubit gate operations a crucial technique is electron spin resonance, which up to now has been demonstrated by only one group [16]. The lack of reproducibility of this experiment partly hinges upon our poor understanding of the electronic structure of SAQDs, and how the g-factor changes by its physical properties. As other key components, on-demand generation of non-classical light sources are needed for cryptology and metrology applications. Due to their discrete energy levels, strong confinement and Coulomb interaction, SAQDs can harbour excitons [17, 18] so that via biexciton-exciton cascade recombination, SAQDs can generate single photon and entangled photon pairs. InGaAs SAQDs show promising results for on-demand single-photon emitters [19, 20, 21]. As a technical note, the transmission of information via fiber optics needs to be in O-band (1310 nm) or C-band (1550 nm) for minimum loss [22, 23]. For this reason, there are intensive on-going research on generating single-photons and polarization-entangled photon pairs that could be transmitted in these bands, and sure enough InGaAs based emitters that are emitting in the C-band are reported for both [24, 25]. To date, the best performance for on-demand generation of polarization-entangled photon pair was shown by Muller *et. al.* [26].

For the quantum information processing, the most important concern is the coherence times of the qubits. Long coherence times of carriers confined in SAQDs makes them good candidates for such applications [9, 10]. Apart from the carrier spins, nuclear spins having transverse coherence times up to a millisecond can be used for information storage [27]. Also, nuclear spins were demonstrated to be good at taming the electron spin coherences [28]. It has been shown that the dynamical decoupling sequences are also effective to increase the coherence time of hole spins while suppressing the nuclear spin background [29, 30].

As the electronic structure of SAQDs depend on shape, size and composition, the fabrication methods have substantial effects. The development and optimization of growth techniques such as molecular beam epitaxy (MBE) [31] and metal organic chemical vapor deposition (MOCVD) [32] allow SAQDs to be grown in

2

high quality. Today, a mode of MBE, Stranski-Krastanov (SK) [33] depicted in Fig. 1.1, is the state-of-art method to grow SAQDs [3]. First, InAs is deposited onto a GaAs substrate as a thin film which forms the so-called wetting layer. If InAs is deposited further, the mismatch between the lattice constants of InAs (6.058 Å) and GaAs (5.653 Å) causes strain to accumulate since lattice constant of InAs is larger than GaAs. In order to minimize the energy, InAs atoms relax and the islands are shaped which are called freestanding SAQDs. If GaAs is deposited on top, they became embedded (also called capped) SAQDs [3, 34, 35]. As the thermodynamic effects are in charge in the growth process [36], the produced SAQDs can have different compositions. Therefore, in order to model these complex structures accurately, atomistic methods are needed along with the experimental transmission electron microscopy and spectroscopic data.
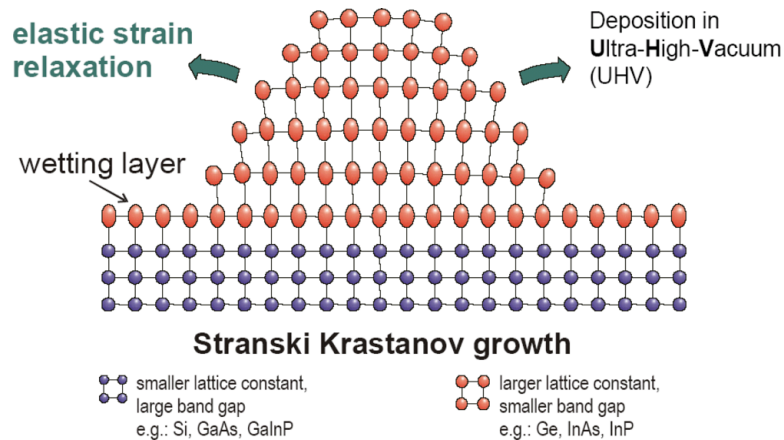
Figure 1.1: The formation of islands in SK mode. The figure is taken from "Self-assembling quantum dots for optoelectronic devices on Si and GaAs", K. Eberl *et.al*, Physica E: Low-dimensional Systems and Nanostructures, vol. 9, no. 1, p. 164–174,2001, Elsevier

1.1   In this thesis

In the light of recently developed semi-empirical pseudopotentials within our group [1], our aim in this thesis is to develop computational atomistic tools for the single-particle electronic structures of these SAQDs having various shapes

and different In/Ga concentrations. In chapter 2, we describe and derive the linear combination of bulk bands (LCBB) method for the calculations of electronic structure [37, 38]. Chapter 3 is devoted to how wave function envelopes can be extracted from LCBB wave functions. Since it is sometimes hard to identify the atomistic wave functions or extracted envelopes, in this chapter we are also demonstrating a method to identify the wave function envelopes with their angular momentum quantum number compositions. Results on electronic structures of InGaAs SAQDs with different shapes, concentration and sizes are presented and discussed in the chapter 4. The chapter 5 offers a self-critique of our approach and the conclusion.

Chapter 2

Electronic structure up to million atoms: Linear combination of bulk bands

To predict the physical properties of the materials or to understand the underlying physics of the these properties, accurate and scalable models are needed. The nanostructures consist of up to million atoms which makes the quantum mechanical calculations hard. These difficulties can be overcome by elegantly thought series of approximations without losing the information needed. In this respect, Wang, Franceschetti and Zunger proposed a technique intended for geometry-independent large-scale atomic electronic structure calculations which exploits the atomic nature of pseudopotentials for describing the crystal potential at the same time leveraging the bulk Bloch bands of the materials for expanding the wave functions, namely "linear combination of bulk bands" (LCBB) [37, 38].

Today, there are a large number of methods to calculate the electronic structure. The most simple of them is the well-known $\mathbf{k} \cdot \mathbf{p}$ method which is used in conjunction with the envelope function approximation (EFA) in the case of nanostructures. To list few of the drawbacks of this method, it takes the geometry of the structure as input since it is a continuum model and also it expands

the wave functions by the envelope functions on the $\mathbf{\Gamma}$-point, thus it cannot generate atomistic results. *Ab-initio* calculations cannot tackle large-scale problems involving several tens of thousands of atoms such as this work because of their computational expenses [39]. Atomistic tight-binding method and LCBB method are two sensible solutions to all of the problems listed above. The only drawback is their non-self-consistent nature which also can be fixed [39].

As mentioned above, LCBB uses the Bloch function basis of the underlying bulk constituents. In principle they are complete which means, for a given bulk material μ (InAs or GaAs for an InGaAs SAQD) we have

$$\int_V \phi_{n,\mathbf{k}}^{\mu}(\mathbf{r})^* \phi_{n',\mathbf{k}'}^{\mu}(\mathbf{r}) d^3 r = \delta_{n,n'} \delta_{\mathbf{k},\mathbf{k}'} \ , \tag{2.1}$$

where n is the bulk band index, $\mathbf{k}$ is the wave vector in first Brillouin zone (BZ) and μ is the material index. This completeness enables us to expand the wave functions of a nanostructure by the Bloch functions

$$\psi^j(\mathbf{r}) = \frac{1}{\sqrt{N}} \sum_{n,\mathbf{k},\mu} C_{n,\mathbf{k}}^{\mu j} \phi_{n,\mathbf{k}}^{\mu}(\mathbf{r}) \ , \tag{2.2}$$

where N is the number of primitive cells in the supercell, $C_{n,\mathbf{k}}^{\mu j}$ is the expansion coefficient. Bloch functions can be expressed as

$$\phi_{n,\mathbf{k}}^{\mu}(\mathbf{r}) = e^{i\mathbf{k}\cdot\mathbf{r}} u_{n,\mathbf{k}}^{\mu}(\mathbf{r}) \ , \tag{2.3}$$

where $u(\mathbf{r})$ is cell-periodic part. This can be expanded as well, in terms of the plane waves of reciprocal lattice vectors $\mathbf{G}$

$$u_{n,\mathbf{k}}^{\mu}(\mathbf{r}) = \frac{1}{\sqrt{\Omega_0}} \sum_{\mathbf{G}} B_{n,\mathbf{k}}^{\mu}(\mathbf{G}) e^{i\mathbf{G}\cdot\mathbf{r}} \ , \tag{2.4}$$

where Ω_0 is the volume of a primitive cell and $B_{n,\mathbf{k}}^{\mu}(\mathbf{G})$ is the expansion coefficient. After combining all of the expansions, the wave function becomes

$$\psi^j(\mathbf{r}) = \frac{1}{\sqrt{V}} \sum_{n,\mathbf{k},\mu} C_{n,\mathbf{k}}^{\mu j} \sum_{\mathbf{G}} B_{n,\mathbf{k}}^{\mu}(\mathbf{G}) e^{i(\mathbf{k}+\mathbf{G})\cdot\mathbf{r}} \ , \tag{2.5}$$

where $V = N\Omega_0$ is the volume of the supercell. Expanding the wave functions by the bulk Bloch functions allows us to choose intuitive basis sets for each

6

material. Its virtue comes from the fact that not all of the bands in BZ contributes to the nanostructure states of interest and with a decisive choice the problem dimensions can be reduced notably so that the large-scale nanostructures can be easily tackled. Therefore, all of the corresponding summations given here are limited to N_B which is number of bands chosen for n, $N_{\mathbf{k}}$ number of chosen bulk wave vectors $\mathbf{k}$. Another approximation that is introduced is the cut-off energy of the reciprocal lattice vectors $\mathbf{G}$ which limits the number of $\mathbf{G}$ to $N_{\mathbf{G}}$.

The single-particle nanostructure Hamiltonian is

$$\hat{H} = \hat{T} + \hat{V}_{xtal} = -\frac{\hbar^2 \nabla^2}{2m_0} + \hat{V}_{xtal} \ , \tag{2.6}$$

where $\hat{T}$ is the kinetic energy, $\hat{V}_{xtal}$ is the crystal potential energy operators, m_0 is the free electron mass. In order to find the energy eigenvalues and wave functions, this needs to be diagonalized. The general eigenvalue equation can be written as

$$\sum_{n,\mathbf{k},\mu} \langle n'\mathbf{k}'\mu' | \hat{T} + \hat{V}_{xtal} | n\mathbf{k}\mu \rangle C_{n,\mathbf{k}}^{\mu j} = E^j \sum_{n,\mathbf{k},\mu} C_{n,\mathbf{k}}^{\mu j} \langle n'\mathbf{k}'\mu' | n\mathbf{k}\mu \rangle \ , \tag{2.7}$$

where E^j is the energy eigenvalue of the state j. The matrix elements of kinetic energy term can be expressed in an open form

$$
\begin{aligned}
\langle n'\mathbf{k}'\mu' | \hat{T} | n\mathbf{k}\mu \rangle = &-\frac{1}{N} \int_V d^3 r \frac{1}{\sqrt{\Omega_0}} \sum_{\mathbf{G}'} \left[B_{n'\mathbf{k}}^{\mu'}(\mathbf{G}') \right]^* e^{-i(\mathbf{k}'+\mathbf{G}')\cdot\mathbf{r}} \\
&\times \frac{\hbar^2 \nabla^2}{2m_0} \frac{1}{\sqrt{\Omega_0}} \sum_{\mathbf{G}} B_{n\mathbf{k}}^{\mu}(\mathbf{G}) e^{i(\mathbf{k}+\mathbf{G})\cdot\mathbf{r}} \ ,
\end{aligned}
\tag{2.8}
$$

where the integral is over the supercell. After taking the derivative and re-expressing the volume (supercell) integral as summation of integrals on all primitive cells, we have

$$
\begin{aligned}
\langle n'\mathbf{k}'\mu' | \hat{T} | n\mathbf{k}\mu \rangle = &\sum_{\mathbf{G},\mathbf{G}'} \left[B_{n'\mathbf{k}'}^{\mu'}(\mathbf{G}') \right]^* B_{n\mathbf{k}}^{\mu}(\mathbf{G}) \frac{\hbar^2 |\mathbf{k}+\mathbf{G}|^2}{2m_0} \\
&\times \underbrace{\frac{1}{N} \sum_j e^{i(\mathbf{k}-\mathbf{k}')\cdot\mathbf{R}_j}}_{\delta_{\mathbf{k},\mathbf{k}'}} \underbrace{e^{i(\mathbf{G}-\mathbf{G}')\cdot\mathbf{R}_j}}_{1} \underbrace{\frac{1}{\Omega_0} \int_{\Omega_0} d^3 r_c e^{i(\mathbf{G}-\mathbf{G}')\cdot\mathbf{r}_c}}_{\delta_{\mathbf{G},\mathbf{G}'}} \\
=&\delta_{\mathbf{k},\mathbf{k}'} \sum_{\mathbf{G}} \left[B_{n'\mathbf{k}'}^{\mu'}(\mathbf{G}) \right]^* B_{n\mathbf{k}}^{\mu}(\mathbf{G}) \frac{\hbar^2 |\mathbf{k}+\mathbf{G}|^2}{2m_0} \ .
\end{aligned}
\tag{2.9}
$$

7

For the crystal potential term, we insert two identities $\hat{I} = \int d^3r \, |\mathbf{r}\rangle \langle\mathbf{r}|$ as

$$\langle n'\mathbf{k}'\mu'| \, \hat{V}_{xtal} \, |n\mathbf{k}\mu\rangle = \int d^3r \int d^3r' \, \langle n'\mathbf{k}'\mu'|\mathbf{r}\rangle \langle\mathbf{r}| \, \hat{V}_{xtal} \, |\mathbf{r}'\rangle \langle\mathbf{r}'|n\mathbf{k}\mu\rangle \ . \qquad (2.10)$$

The pseudopotentials we are using are local, therefore we have

$$\langle\mathbf{r}| \, \hat{V}_{xtal} \, |\mathbf{r}'\rangle = \delta(\mathbf{r} - \mathbf{r}')V_{loc}(\mathbf{r}) \ , \qquad (2.11)$$

where V_{loc} is the total of local and spherically symmetric atomic pseudopotentials. Putting this into Eq. 2.10 makes the primed integral to drop due to Dirac delta,

$$\langle n'\mathbf{k}'\mu'| \, \hat{V}_{xtal} \, |n\mathbf{k}\mu\rangle = \int d^3r \, \langle n'\mathbf{k}'\mu'|\mathbf{r}\rangle V_{loc}(\mathbf{r}) \langle\mathbf{r}|n\mathbf{k}\mu\rangle \ . \qquad (2.12)$$

V_{loc} can be expressed as a summation of atomic pseudopotentials. So, the matrix elements becomes

$$\langle n'\mathbf{k}'\mu'| \, \hat{V}_{xtal} \, |n\mathbf{k}\mu\rangle = \frac{1}{N\Omega_0} \sum_{\mathbf{G},\mathbf{G}'} \left[B_{n'\mathbf{k}'}^{\mu'}(\mathbf{G}')\right]^* B_{n\mathbf{k}}^{\mu}(\mathbf{G})$$
$$\times \int_V d^3r \, e^{i(\mathbf{k}+\mathbf{G}-\mathbf{k}'-\mathbf{G}')\cdot\mathbf{r}} \sum_{j,\alpha,\mu''} W_{\alpha}^{\mu''}(\mathbf{R}_j) v_{\alpha}^{\mu''}(\mathbf{r} - \mathbf{R}_j - \mathbf{d}_{\alpha}^{\mu''}). \qquad (2.13)$$

where $v_{\alpha}^{\mu}(\mathbf{r} - \mathbf{R}_j - \mathbf{d}_{\alpha}^{\mu})$ is the spherically symmetric screened atomic pseudopotential for atom/basis α, $\mathbf{R}_j$ is the position vector pointing to the primitive cell j and $\mathbf{d}_{\alpha}^{\mu}$ is the position vector of basis α of material of type μ. $W_{\alpha}^{\mu}(\mathbf{R}_j)$ is the weight function which selects atom/basis α of material μ on the position $\mathbf{R}_j + \mathbf{d}_{\alpha}^{\mu}$ and usually takes the discrete values of $[0,1]$. We can set the origin to the center of the each atom/basis by a change of variable $\mathbf{r}$ as $\mathbf{r} \to \mathbf{R}_j + \mathbf{r}_c + \mathbf{d}_{\alpha}^{\mu''}$ which yields after reordering the terms

$$\langle n'\mathbf{k}'\mu'| \, \hat{V}_{xtal} \, |n\mathbf{k}\mu\rangle = \sum_{\mathbf{G},\mathbf{G}'} \left[B_{n'\mathbf{k}'}^{\mu'}(\mathbf{G}')\right]^* B_{n\mathbf{k}}^{\mu}(\mathbf{G}) \sum_{\mu''} \frac{1}{\Omega_0} \sum_{\alpha} e^{i(\mathbf{k}+\mathbf{G}-\mathbf{k}'-\mathbf{G}')\cdot\mathbf{d}_{\alpha}^{\mu''}}$$
$$\times \int_{\Omega_0} v_{\alpha}^{\mu''}(\mathbf{r}_c)e^{i(\mathbf{k}+\mathbf{G}-\mathbf{k}'-\mathbf{G}')\cdot\mathbf{r}_c} \frac{1}{N} \sum_{j} W_{\alpha}^{\mu''}(\mathbf{R}_j)e^{i(\mathbf{k}-\mathbf{k}')\cdot\mathbf{R}_j} \ . \qquad (2.14)$$

The last summation is basically a Fourier series which we can denote as

$$\mathcal{W}_{\alpha}^{\mu}(\mathbf{k} - \mathbf{k}') = \sum_{j} W_{\alpha}^{\mu''}(\mathbf{R}_j)e^{i(\mathbf{k}-\mathbf{k}')\cdot\mathbf{R}_j} \ . \qquad (2.15)$$

Since the pseudopotentials are localized to the vicinity of the atomic sites, the integral on the right hand side of Eq. 2.14 can be extended over all space as the potentials will die out quickly. With the appropriate coefficients, it becomes a Fourier transform which can be denoted as

$$\mathcal{V}_\alpha^{\mu''}(|\mathbf{k} + \mathbf{G} - \mathbf{k}' - \mathbf{G}'|^2) = \frac{1}{\chi_0} \int_{-\infty}^{\infty} v_\alpha^{\mu''}(\mathbf{r}_c) e^{i(\mathbf{k}+\mathbf{G}-\mathbf{k}'-\mathbf{G}')\cdot\mathbf{r}_c} , \qquad (2.16)$$

where $\chi_0 = \Omega_0/N_{\mu''}$ and $N_{\mu''}$ is the number of atoms/basis in the primitive cell. So, we have

$$\langle n'\mathbf{k}'\mu'| \hat{V}_{xtal} |n\mathbf{k}\mu\rangle = \sum_{\mathbf{G},\mathbf{G}'} B_{n\mathbf{k}}^{\mu}(\mathbf{G}) \left[B_{n'\mathbf{k}'}^{\mu'}(\mathbf{G}')\right]^*$$

$$\times \sum_{\mu'',\alpha} \frac{1}{N_{\mu''}} \mathcal{V}_\alpha^{\mu''}(|\mathbf{k} + \mathbf{G} - \mathbf{k}' - \mathbf{G}'|^2) \qquad (2.17)$$

$$\times \mathcal{W}_\alpha^{\mu''}(\mathbf{k} - \mathbf{k}') e^{-i(\mathbf{k}+\mathbf{G}-\mathbf{k}'-\mathbf{G}')\cdot\mathbf{d}_\alpha^{\mu''}} .$$

In the light of this derivation, the overlap term on the right hand side of Eq. 2.7 can be reduced to

$$\langle n'\mathbf{k}'\mu'|n\mathbf{k}\mu\rangle = \delta_{k,k'} \sum_{\mathbf{G}} \left[B_{n'\mathbf{k}'}^{\mu'}(\mathbf{G})\right]^* B_{n\mathbf{k}}^{\mu}(\mathbf{G}) . \qquad (2.18)$$

The spin-orbit interaction (SOI) can be described by the Hamiltonian [40, 41],

$$\hat{H}_{SO} = \sum_{\ell=1}^{\infty} |\ell\rangle V_{SO,\ell}(r) \vec{\ell} \cdot \vec{\sigma} \langle\ell| , \qquad (2.19)$$

where $V_{SO,\ell}(r)$ is the nonlocal SOI potential which arises from the relativistic effects of core electron states, ℓ is the orbital angular momentum and $\vec{\sigma}$ is the Pauli spin matrix. The matrix elements of this Hamiltonian in a plane-wave basis, taking only $\ell = 1$ can be written as

$$\langle s, \mathbf{K}| \hat{H}_{SO} |s', \mathbf{K}'\rangle = -i \langle s| \vec{\sigma} |s'\rangle \left[12\pi \frac{\mathbf{K} \times \mathbf{K}'}{KK'} V_{\ell=1}^{SO}(\mathbf{K}, \mathbf{K}')\right] ,$$

where $\mathbf{K} = \mathbf{k} + \mathbf{G}$, $|s\rangle$ is the spin vector for spin-up and down and $S(\mathbf{K}' - \mathbf{K})$ is the structure factor of bulk crystal. $V_\ell^{SO}(\mathbf{K}, \mathbf{K}')$ is

$$V_\ell^{SO}(\mathbf{K}, \mathbf{K}') = \int_0^\infty \frac{dr}{\Omega_0} r^2 j_\ell(Kr) V_\ell^{SO}(r) j_\ell(K'r) , \qquad (2.20)$$

where j_ℓ is the spherical Bessel function of the first kind. Here, $V_\ell^{SO}(r)$ is taken as a Gaussian function.
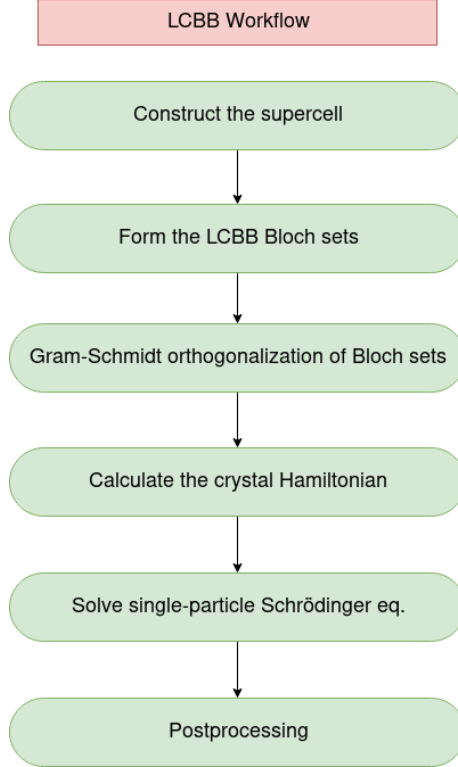
Figure 2.1: Workflow of LCBB method to calculate atomistic electronic structure of a nanostructure.

In this work, the semi-empirical pseudopotential parameters for InAs and GaAs are taken from Çakan *et.* *al.* [1] and given in Table 2.1. The advantages of using these parameters are the pseudopotential form factors were obtained after tuning the local density approximation (LDA) results so that they can generate quality wave functions, the pseudopotentials are cleared from non-local parts of the potential, they can reproduce the band edges calculated by density functional theory with various deformation potentials accurately and they are fitted to be used in large-scale atomic calculations with an energy cut-off of 5 Ry.

Local form factors	$GaAs$	$InAs$	Slopes for PCHIP	$GaAs$	$InAs$
V_0^s	-0.6421	-0.5469	s_0^s	0.0000	0.0000
$V_{\sqrt{3}}^s$	-0.2350	-0.2070	$s_{\sqrt{3}}^s$	0.0699	-0.1760
$V_{\sqrt{8}}^s$	0.0150	0.0000	$s_{\sqrt{8}}^s$	0.1250	0.1250
$V_{\sqrt{1}}^s$	0.0729	0.0465	$s_{\sqrt{1}}^s$	0.0596	-0.0062
V_0^a	-0.1040	-0.0880	s_0^a	0.0000	0.0000
$V_{\sqrt{3}}^a$	0.0760	0.0540	$s_{\sqrt{3}}^a$	0.0250	-0.0350
$V_{\sqrt{4}}^a$	0.0570	0.0466	$s_{\sqrt{4}}^a$	-0.1150	-0.0900
$V_{\sqrt{1}}^a$	0.0061	0.0070	$s_{\sqrt{1}}^a$	-0.0100	-0.0220
Asymptotic parameters			**Hydrostatic strain parameter**		
a_5	4.05	4.50	γ	-1.7392	-0.1046
a_6	0.39	0.41	**Spin-orbit coupling parameter (Ry)**		
Cut-off energy (Ry)			λ_S	0.0213	0.0205
$E_{cut-off}$	5.00	4.85			

Table 2.1: Semi-empirical pseudopotential parameters for InAs and GaAs used in this work. "PCHIP" stands for "piecewise cubic Hermite interpolating polynomial". The table is taken from Ref. [1].

An important aspect of our calculations is the strain. Naturally, the positions of the atoms in InGaAs SAQD are not in their ordered zinc-blende sites due to relaxation of stress so that to use the fast Fourier transform relies on an ordered lattice and additional approximations and tables are needed as in Ref. [38]. In this work, we are not employing this cumbersome approach by using the original (disordered or ordered) lattice sites, while being content with the discrete Fourier transform.

Chapter 3

Wave function analysis of InAs quantum dots

For the characterization of atomistic wave functions of any nanostructure, 3D isosurface plots are not sufficient. For alloy QDs such as $In_xGa_{1-x}As$ or for spherical cut-plane QDs (hydrophobic, half sphere or lens) polar symmetry is broken and thus, the wave functions will have a mixed characteristic in terms of angular momentum. This mixing could only be understood by detailed wave function analysis. However, in LCBB formalism, as in any atomistic approach, calculating angular momentum projections of an atomistic wave function is not an easy task due to the fast oscillations of the cell-periodic part as sketched in the Fig. 3.1. These oscillations are the main obstacle for this task and must be somehow gotten rid of. There is a simple remedy in the literature for this kind of oscillations of the wave functions. It is the famous envelope function approximation. This approximation can, in principle, be used to calculate LCBB wave function envelopes. In this chapter, two envelope extraction methods and the angular momentum projection calculations of a wave function envelope was discussed.
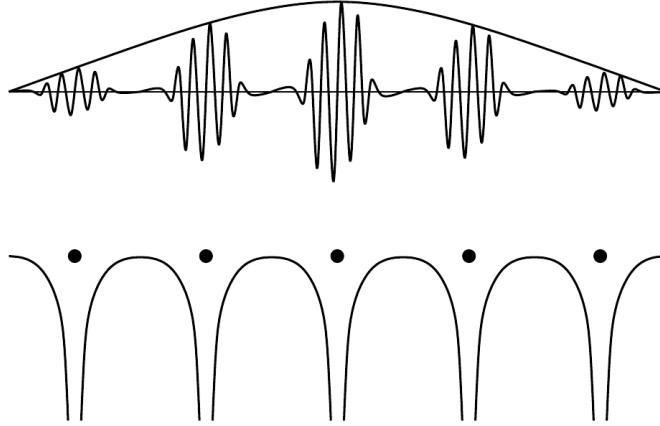
Figure 3.1: Due to the ionic potential of the atomic sites (below part), the wave function wiggles (upper part). The line at the top is the slowly varying envelope. The figure is taken from "*Spin-orbit coupling effects in two-dimensional electron and hole systems*", Roland Winkler, Springer, 2010.

3.1 Envelope extraction methods

3.1.1 Gaussian smoothing

In image and signal processing, Gaussian smoothing (i.e filter) is an established tool. It can simulate blur effect on an image and it can be useful for edge detection. In signal processing it is used for suppressing white noise [42]. As the Fourier transform of a Gaussian is also a Gaussian, this property can be very useful. A Gaussian filter is a Gaussian function which is defined as

$$g(x) = \frac{1}{\sqrt{2\pi}\sigma} e^{-x^2/2\sigma^2} \ , \tag{3.1}$$

where σ is the standard deviation and it governs how strong the filter acts on the function. Due to its spatial separability, this filter can be applied in 3D through convolution and it smooths out the oscillations. For the oscillating isosurfaces, the filter acts nicely and returns envelope-like isosurfaces. Increasing σ, increases the smoothness of the isosurfaces. However, this freedom in σ cannot generate

definite isosurfaces. Furthermore, the grid density also effects the isosurfaces. Denser grids may need higher values of σ since the oscillations would be more prominent.

The definition of an envelope function can vary as long as it filters out the high frequency oscillations which makes this method legitimate. However, in terms of performance and robustness, this method could be problematic. Still, since it is computationally very cheap, it may be used if the purpose is to have a general idea about the behavior of a wave function. Fig. 3.2 shows the same wave function envelopes generated by using this method for two different σ values.
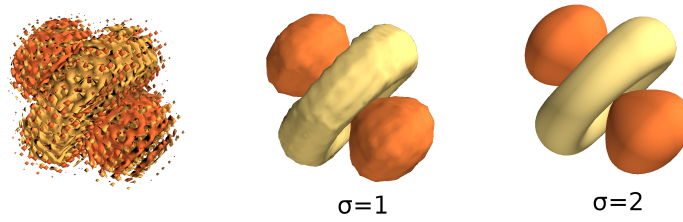

Figure 3.2: An atomistic wave function (left) and its envelopes after applying Gaussian filter with different σ values.

3.1.2   Envelope function approximation in LCBB

Envelope function approximation suggests that a wave function can be expanded in terms of the periodic part of the Bloch function at a given wave-vector, for example $\mathbf{\Gamma}$ high-symmetry point for our case.

$$\psi(\mathbf{r}) = \sum_{n}^{\infty} f_n(\mathbf{r}) u_{n,\mathbf{\Gamma}}(\mathbf{r}) \ . \tag{3.2}$$

The function $f_n(\mathbf{r})$ is the so-called envelope function which corresponds to the contribution of bulk band index n to the whole wave function. Our aim here is to find this envelope function within the LCBB formalism. Equating the wave

function above with the LCBB wave function given in Eq. 2.5

$$\psi(\mathbf{r}) = \sum_n f_n(\mathbf{r}) u_{n,\mathbf{\Gamma}}(\mathbf{r}) \tag{3.3}$$

$$= \frac{1}{\sqrt{N}} \sum_{n,\mathbf{k},\mu} C_{n,\mathbf{k}}^{\mu,j} e^{i\mathbf{k}\cdot\mathbf{r}} u_{n,\mathbf{k}}^{\mu}(\mathbf{r}) \ . \tag{3.4}$$

The plane-wave (exponential) part on the right hand side of the equation is responsible for the slowly-varying oscillations and the cell-periodic part is responsible for the fast oscillations. To be able to suppress the fast oscillations, we project the wave function to Γ-point. Multiplying both sides with $[u_{n\mathbf{\Gamma}}]^*$ and taking the integral over all space we get,

$$\sum_n \int f_n(\mathbf{r}) u_{n,\mathbf{\Gamma}}^{\mu}(\mathbf{r}) \left[u_{n,\mathbf{\Gamma}}^{\mu}(\mathbf{r})\right]^* d^3r = \frac{1}{\sqrt{N}} \sum_{n,\mathbf{k}} C_{n,\mathbf{k}}^{\mu,j} \int e^{i\mathbf{k}\cdot\mathbf{r}} u_{n,\mathbf{k}}^{\mu}(\mathbf{r}) \left[u_{n,\mathbf{\Gamma}}^{\mu}(\mathbf{r})\right]^* d^3r \ . \tag{3.5}$$

As the envelope function and the plane-wave part is slowly varying with respect to the cell-periodic part, we assume that they are constant within a unit cell, then they can be taken out of the integral. Using the orthogonality of Bloch functions, envelope function is found to be

$$\sum_n f_n(\mathbf{r}) = \frac{1}{\sqrt{N}} \sum_{n,\mathbf{k},\mu} C_{n,\mathbf{k}}^{\mu,j} e^{i\mathbf{k}\cdot\mathbf{r}} \delta_{\mathbf{k},\mathbf{\Gamma}} \sum_{\mathbf{G}} B_{n,\mathbf{k}}^{\mu}(\mathbf{G}) \left[B_{n,\mathbf{\Gamma}}^{\mu}(\mathbf{G})\right]^*. \tag{3.6}$$

Taking care of the summation on the left hand side, the equation

$$f^j(\mathbf{r}) = \frac{1}{\sqrt{N}} \sum_{n,\mathbf{k},\mu} C_{n,\mathbf{k}}^{\mu,j} e^{i\mathbf{k}\cdot\mathbf{r}} \delta_{\mathbf{k},\mathbf{\Gamma}} \sum_{\mathbf{G}} B_{n,\mathbf{k}}^{\mu}(\mathbf{G}) \left[B_{n,\mathbf{\Gamma}}^{\mu}(\mathbf{G})\right]^* \ , \tag{3.7}$$

gives the envelope function for the state j. Fig. 3.3 shows the extracted envelope by this method.
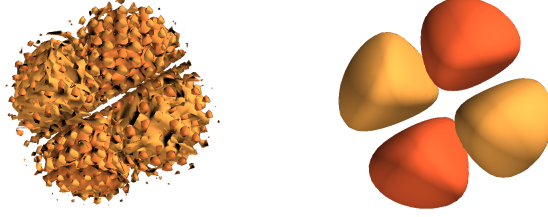
Figure 3.3: Atomistic wave function (left) and the extracted envelope function through envelope function approximation (right) for a QD state.

3.2 Angular momentum decomposition of envelopes

On the unit sphere, any square-integrable function of θ and ϕ can be expanded in terms of spherical harmonics [43] as

$$g(\theta,\phi) = \sum_{\ell=0}^{\infty} \sum_{m=-\ell}^{\ell} c_{\ell m} Y_{\ell m}(\theta,\phi) \ , \tag{3.8}$$

where $c_{\ell m}$ is denoting the expansion coefficients, l is the orbital angular momentum quantum number and m is the magnetic quantum number. However, unlike the function $g(\theta,\phi)$, wave function envelopes depend on r so that the expansion coefficients $c_{\ell m}$ will be r-dependent. Also, the wave equation is separable in spherical coordinates [44] so that the envelopes can be separated with the r-dependence [45] as

$$f(r,\theta,\phi) = \sum_{\ell,m} R_{\ell m}(r) Y_{\ell m}(\theta,\phi). \tag{3.9}$$

The coefficients $R_{lm}(r)$ are

$$R_{\ell m}(r) = \int_0^{2\pi} \int_0^{\pi} d\phi d\theta \sin(\theta) Y_{\ell m}^*(\theta,\phi) f(r,\theta,\phi) \ . \tag{3.10}$$

16

To be able to calculate this integral in spherical coordinates Lebedev quadrature of order 131 which corresponds to 5810 point-grid is used. This grid is designed by Lebedev and Laikov so that it has octahedral rotation and inversion symmetry. Lebedev quadrature gives the best numerical results for these type of spherical integrals where the spherical harmonics are involved since the point weights are determined to solve integrals of spherical harmonics exactly up to some order ℓ [46].

There are two paths that could be taken from here, calculating the change in the compositions for linearly varying the radius and sampling Lebedev grids inside the QD or we can calculate a weight which indicates the relative compositions for the whole QD. As the former harbors much more information, it would be much more effective to understand the characteristics of wave function envelopes than the weights, the latter is simply the integral of the former. For the former for each Lebedev grid, we calculate the compositions of angular momentum quantum numbers as

$$b_\ell(r) = \frac{\sum_m |rR_{\ell m}(r)|^2}{\sum_{\ell=0}^{6} \sum_m |rR_{\ell m}(r)|^2} \ . \tag{3.11}$$

As we can only calculate this up to a certain values of ℓ instead of infinity for the denominator, the result will yield some truncation error. As the wave functions we are dealing with do not have any values of ℓ higher than 4 or at maximum 5, this truncation error will be relatively small if ℓ is taken higher than these values.

The expression that gives the weight is [45]

$$w_\ell = \sum_{m=-\ell}^{\ell} \int_0^{D/2} |rR_{\ell m}(r)|^2 dr \ , \tag{3.12}$$

where D is the diameter of the QD.

As a showcase, Fig. 3.4 shows the r-dependent orbital angular momentum compositions of the wave function envelopes of the spherical $In_{0.25}Ga_{0.75}As$ SAQD of which the energy levels are given in Fig. 4.1(b).
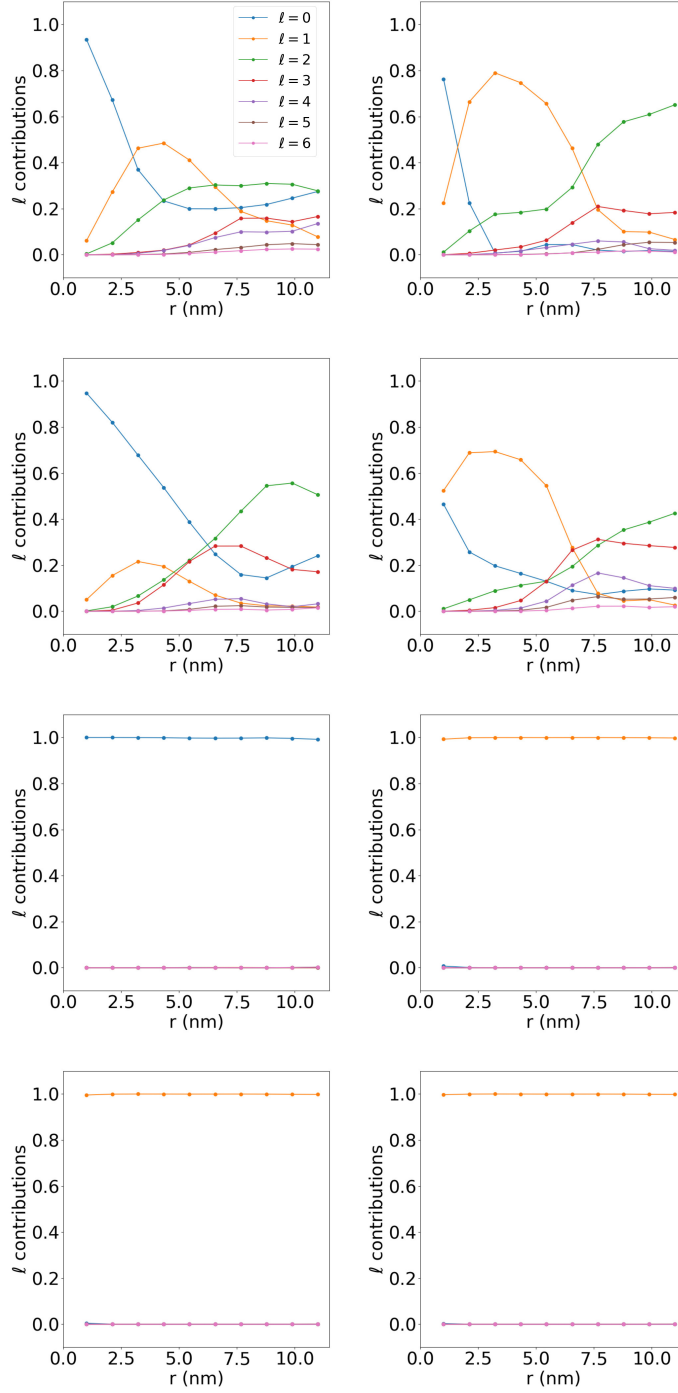
Figure 3.4: The orbital angular momentum compositions of the envelope functions of the four valence states (first four figures) with the highest energies and four conduction states (last four) with the lowest energies of spherical $In_{0.25}Ga_{0.75}As$. The energy levels of this SAQD is given in Fig. 4.1(b). State energies are in the increasing order from top-left to bottom-right.

Chapter 4

Results

In this chapter, we present single-particle electronic bound-states for five different $In_xGa_{1-x}As$ SAQDs. First, the calculation details are discussed. Then, the results are presented while comparing the size, shape and concentration effects.

4.1   Calculational details

The electronic structure calculations are done by using a parallelepiped supercell which is chosen big enough to prevent interactions between periodic image QDs. As a matter of fact, for the lens structure, we also checked with a supercell larger than the one that we used in our calculations and observed that the results did not change by more than 10 meV which can be taken as a typical accuracy measure of our results. The supercell is filled by using two-atom basis. The alloying is done by distributing the gallium atoms in place of indium atoms randomly according to the intended molar fraction of of the QD.

The k-grid from which the bulk basis states are chosen is taken as $9 \times 9 \times 9$ rectangular mesh near the $\boldsymbol{\Gamma}$ high-symmetry point (the center of the mesh). Also, in the literature near $\boldsymbol{\Gamma}$-centered mesh is used for InGaAs SAQDs [47, 45]. The bands that are chosen are between the band indices $3 - 16$ including the spin

degenerate bands and bulk bands of both matrix (GaAs) and core constituents (InAs) with the total number of 28 bands.

As the calculations produce significant amount of surface states owing to bulk bands of matrix material, these are cleaned with the help of a filter that checks whether the state is core-derived or not in accordance with the condition [48]

$$\sum_{n,\mathbf{k}} \left| C_{n,\mathbf{k},j}^{\mathrm{GaAs}} \right|^2 \leq \mathcal{F} \sum_{n,\mathbf{k}} \left| C_{n,\mathbf{k},j}^{\mathrm{InAs}} \right|^2 , \tag{4.1}$$

where $C_{n,\mathbf{k},j}^{\mu}$ are the wave function expansion coefficients (see Eq. 2.5) and $\mathcal{F}$ is the filtering parameter which is taken as 0.1 for all of the calculations here. An example of unfiltered and filtered electronic structures are given in Fig. 4.1(a,b).

The SAQDs in consideration have spherical, hydrophobic and lens geometries. The number of atoms in the supercell is 476 656 for each SAQD. The hydrophobic and the lens shapes are cut out by a plane from the spherical one. Normal vector of this plane has a polar angle of 54.7°. It should be noted that this choice of plane is arbitrary. The spherical QD has a diameter of 10.75 nm and consists of 28 708 atoms. The diameter of the cut-plane of hydrophobic is about 9.3 nm and this QD consists of 24 234 atoms. Lens shaped QDs have a diameter of about 10.5 nm, their height correspond to 4.3 nm and contains 10 116 atoms.

Due to the 6.7% lattice mismatch between InAs and GaAs and since the lattice constant of GaAs is imposed all throughout the structure, the indium atoms are under a hydrostatic compressive strain. Here, we do not relax the atoms so that their atomic positions are in zinc-blende order.

4.2 Size and shape effects on electronic structure

To investigate the effects of the size and the shape, single-particle electronic structure of SAQDs with different geometries having the same indium mole fractions

$x = 0.25$ are presented. The wave functions and their extracted envelopes are shown in Figs. 4.2,4.3,4.4.

As the nanostructure sizes get smaller, the quantum confinement will be more prominent and the HOMO (Highest Occupied Molecular Orbital)-LUMO (Lowest Unoccupied Molecular Orbital) gap will open up. This is called quantum size effect. This effect can be seen easily by comparing the energy gaps (E_{gap}) of given electronic structures. From spherical to lens, the number of QD atoms are getting reduced, therefore, E_{gap} increases while the number of bound states decrease from spherical to lens geometries.

Change in the shape and size, drastically affects the valence state wave functions and their envelopes as expected from the strong mixing among the valence band states. For the conduction states, these changes are not as pronounced as in the valence states. If we concentrate on the so-called p-shell of the conduction states: for the spherical QD the small energy splitting among the three originates from the underlying crystallographic direction variations, whereas for hydrophobic and lens QD cases the third p-states becomes energetically pushed out significantly, as expected from the orientation of cutting plane.
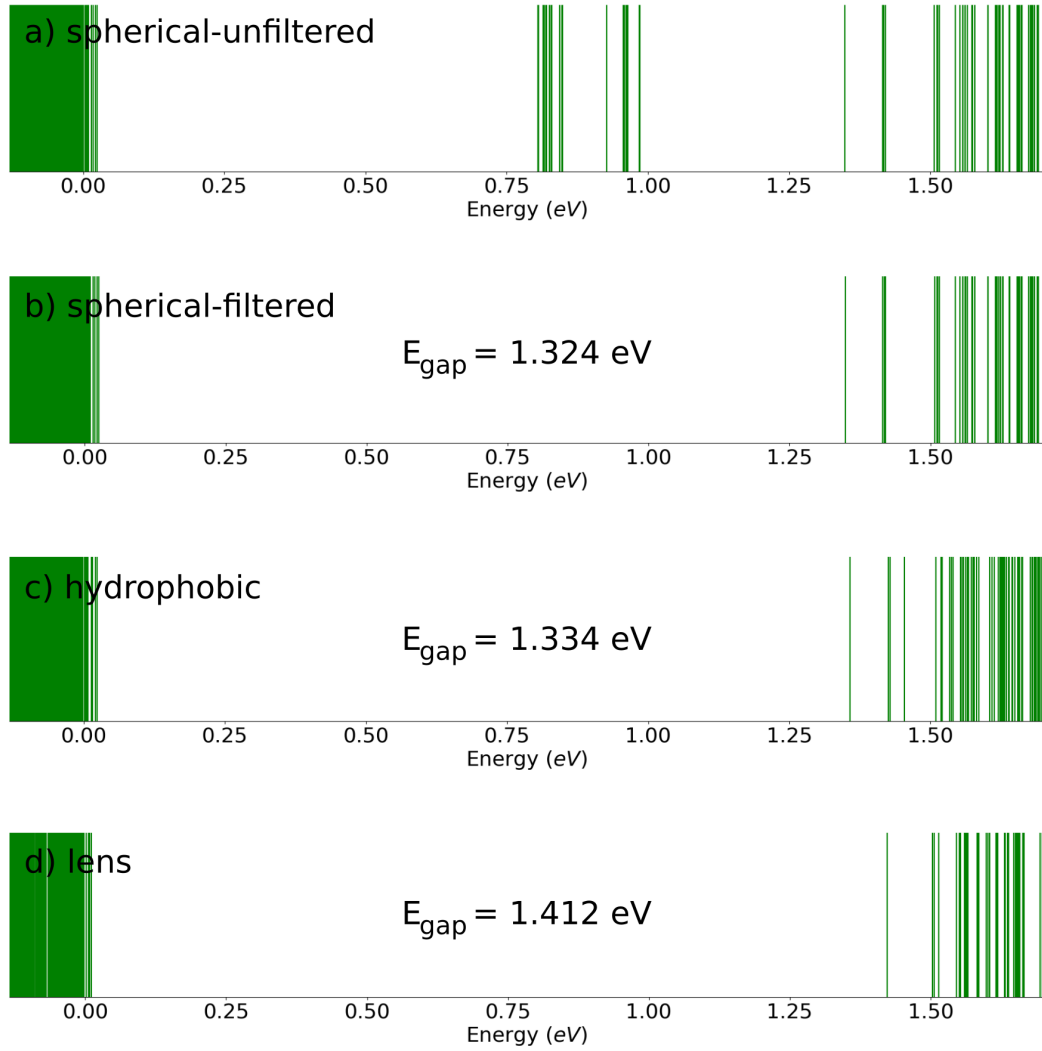
Figure 4.1: Energy levels of an electron in (a, b) spherical, (c) hydrophobic and (d) lens shaped $In_{0.25}Ga_{0.75}As/GaAs$ SAQD. The state energies are relative to the valence band maximum of the bulk GaAs under spin-orbit interaction which is taken to be zero.
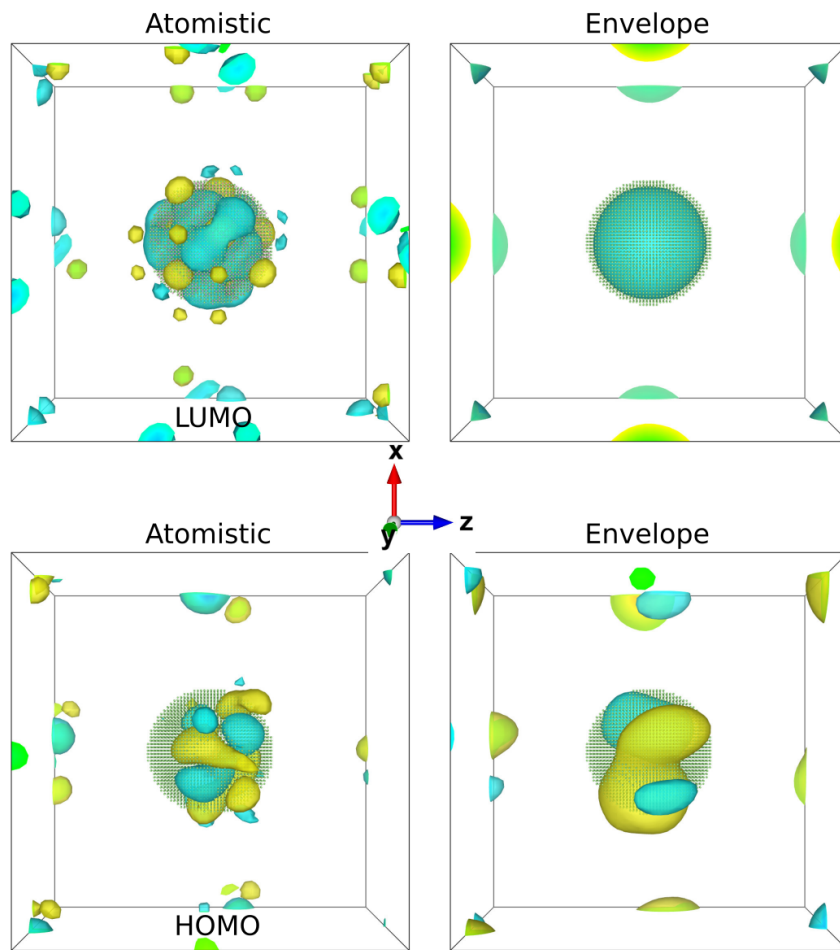
Figure 4.2: Atomistic wave functions and their extracted envelopes for HOMO and LUMO of the spherical $In_{0.25}Ga_{0.75}As/GaAs$ SAQD. The wave functions and envelope isosurfaces are at a confidence interval of 99%. The green dots are in the positions of arsenic atoms of the QD.
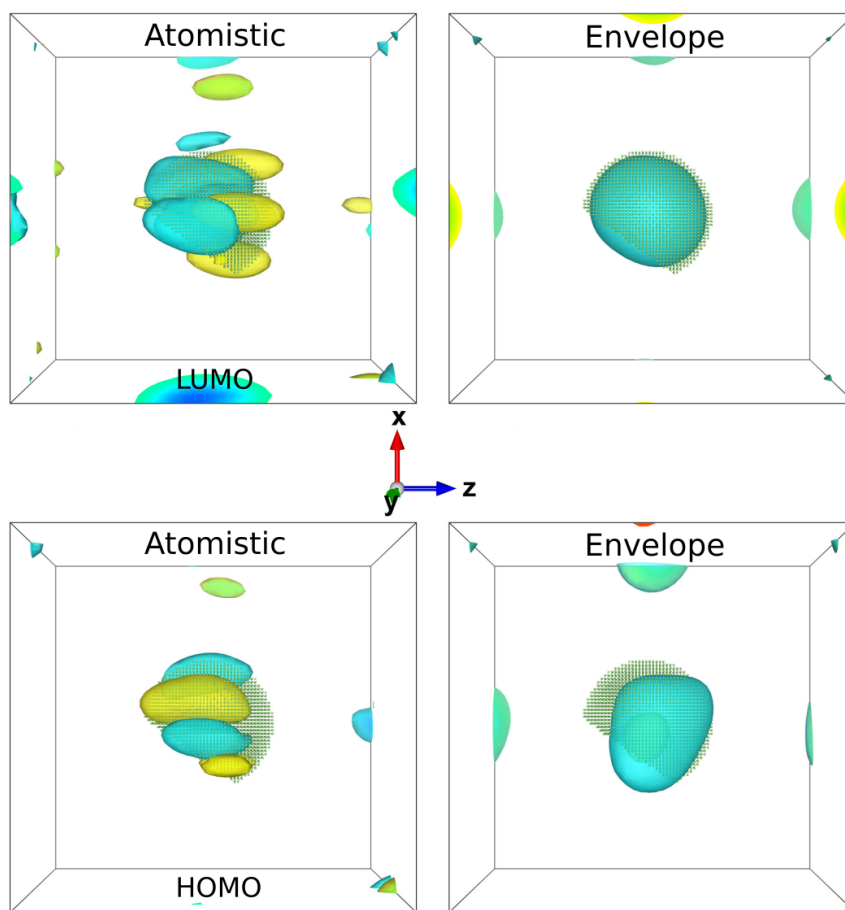
Figure 4.3: Same as the previous figure but for a QD with hydrophobic geometry.

As a note, the atomic nature of the wave functions cannot be seen due to the chosen grid size for the figures for spherical and hydrophobic QDs. A much more denser grid could be used with a price of more computational expense, if it is necessary to see the fast oscillations.
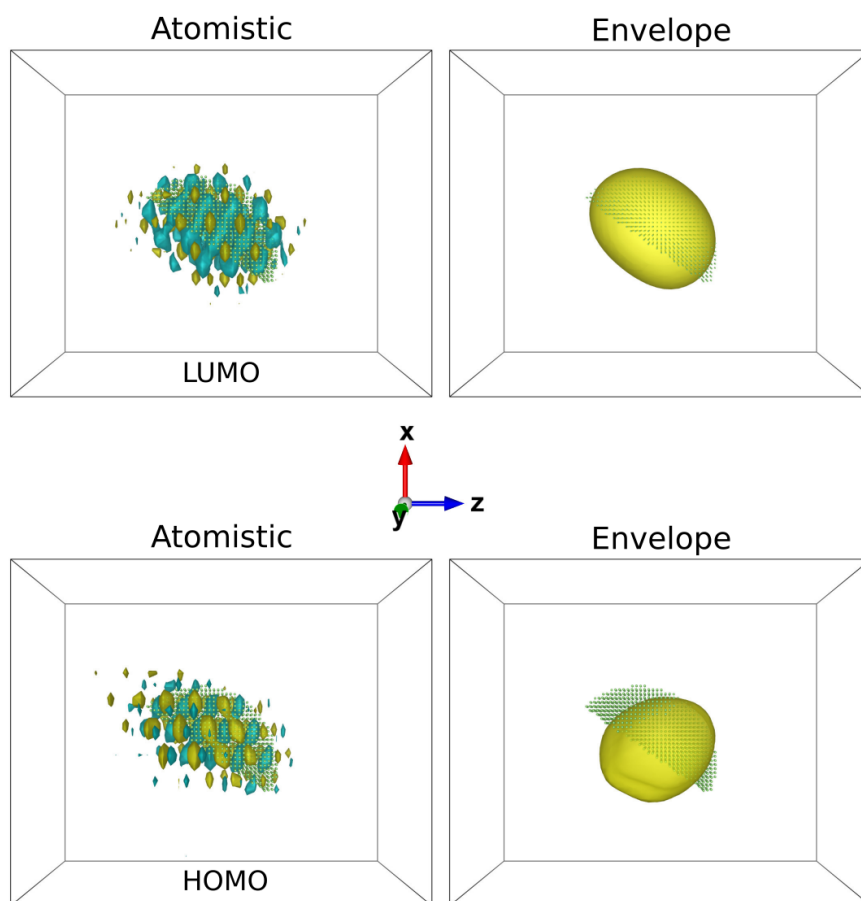
Figure 4.4: Same as the previous figure but for a QD with lens geometry.

4.3 Effect of indium molar fraction

As there is a band gap difference between bulk InAs and GaAs, electronic structure will highly depend on the concentration of these constituents. Electronic structures of SAQDs having the same geometry but different molar fractions are presented in Figs. 4.4,4.6,4.7.
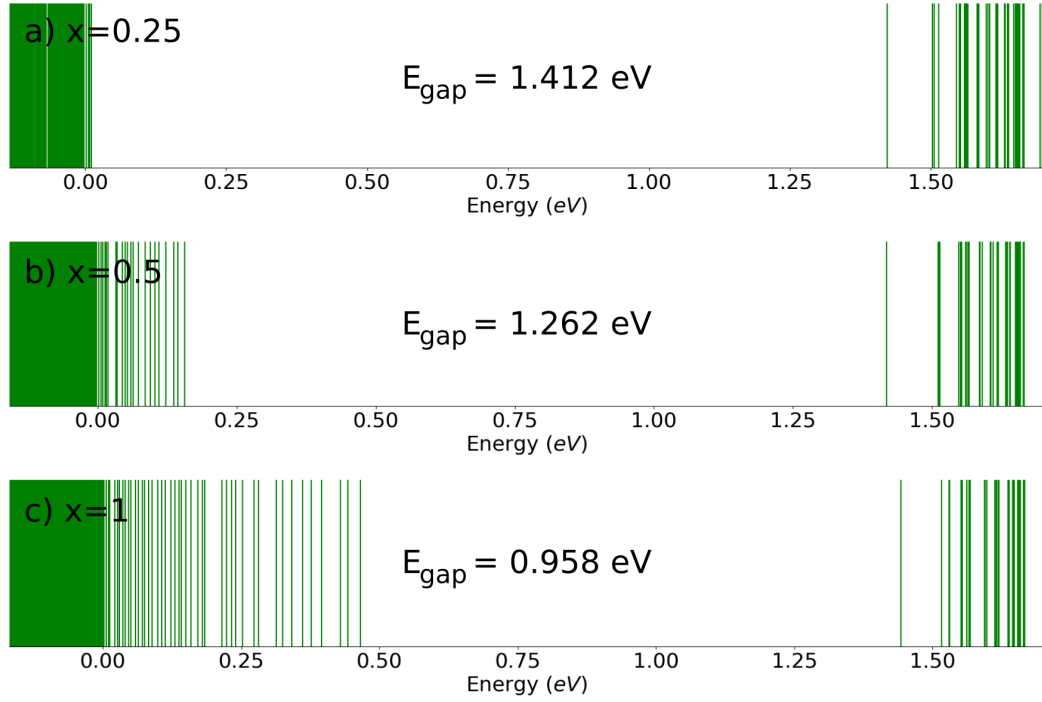
Figure 4.5: Energy levels of an electron in lens shaped In$_x$Ga$_{x-1}$As SAQDs for (a) $x = 0.25$, (b) $x = 0.5$ and (c) $x = 1$.

Comparing the figures, the most pronounced differences are in the E_{gap}. Increasing the mole fraction of indium, decreases the HOMO-LUMO gap which corroborates with the smaller band gap of InAs compared to GaAs. There are slight changes in the LUMO energies but the valence state energies increase greatly with increasing indium molar fraction. Also, the number of valence states increase as the molar fraction of indium increases.
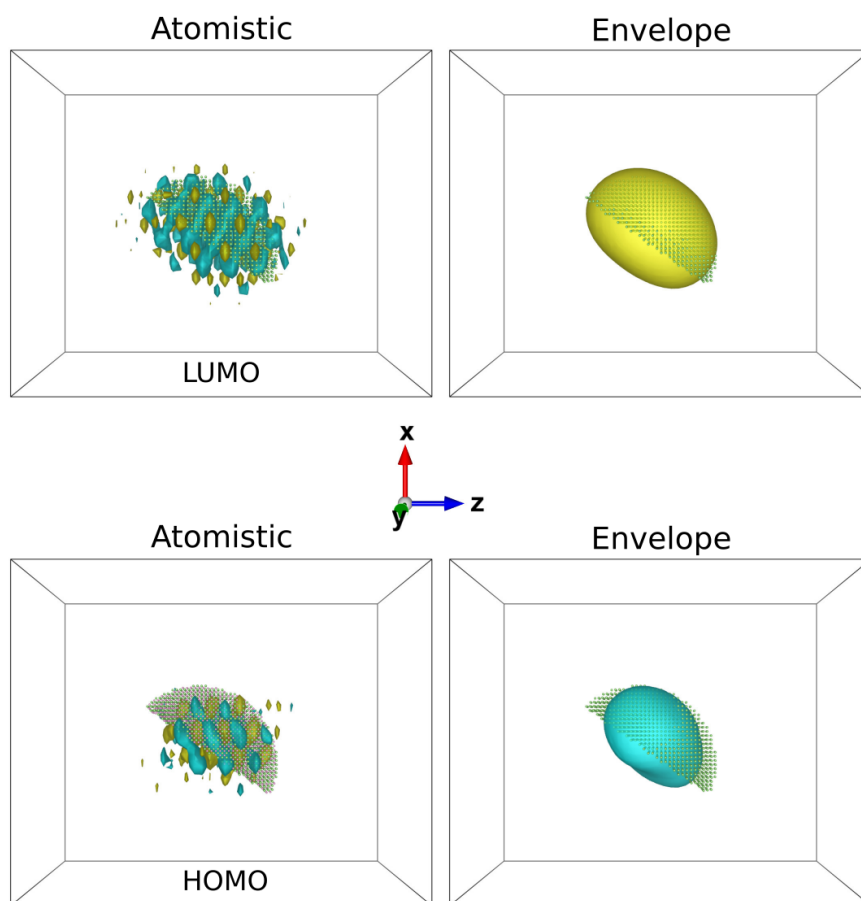
Figure 4.6: Same as the Fig. 4.4 but for $In_{0.5}Ga_{0.5}As/GaAs$ SAQD.

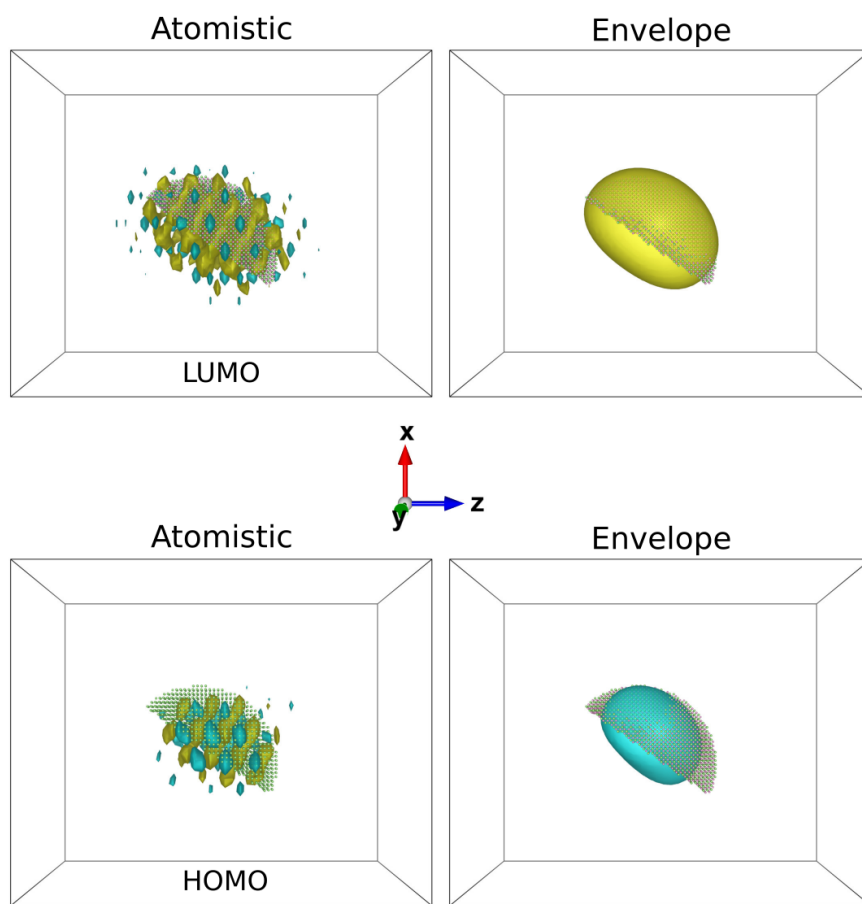Figure 4.7: Same as the previous figure but for pure InAs/GaAs SAQD.

Chapter 5

Conclusion and a self-critique

A large-scale atomistic electronic structure calculations of five different $In_xGa_{1-x}As$ SAQDs were presented and compared. Specifically, the effects of size, shape and indium concentration on the electronic structures of these SAQDs under the hydrostatic compressive strain were examined. As the isosurfaces for atomistic wave functions can be hard to interpret due to their fast oscillating behaviors, two methods for extracting the envelopes were shown in detail. Also, a technique to calculate the orbital angular momentum quantum number compositions of envelopes were discussed.

The electronic structures were calculated by employing linear combination of bulk bands method which is a non-self-consistent method. The self-consistency can be implemented at the expense of additional coding as well as increased computational budget. The ionic relaxation of stress of the supercells were not taken into account. It is an important effect which changes the strain profiles of the QDs, therefore, it affects the electronic structure. Also, the non-self-consistent nature and the necessity for the physical intution-based choice of basis states render the use of the technique more of an art than pure brute computational force.

As a possible future work, the electronic structures of InGaAs SAQDs with

relaxed atoms can be calculated. Also, in connection to QD spin-qubits g-factors of carriers of an InGaAs SAQDs can be calculated using this atomistic approach, as it could shed some light on the underlying reason for the electron spin resonance experiment not being reproducible [16].

Bibliography

[1] A. Çakan, C. Sevik, and C. Bulutay, "Strained band edge characteristics from hybrid density functional theory and empirical pseudopotentials: Gaas, gasb, inas and insb," *Journal of Physics D: Applied Physics*, vol. 49, no. 8, p. 085104, 2016.

[2] D. Bimberg, M. Grundmann, and B. Dieter, *Quantum dot heterostructures.* Wiley, 2001.

[3] P. M. Petroff, "Epitaxial growth and electronic structure of self-assembled quantum dots," in *Single Quantum Dots: Fundamentals, Applications and New Concepts* (P. Michler, ed.), ch. 01, Springer Berlin Heidelberg, 2014.

[4] P. Yu, *Fundamentals of Semiconductors: Physics and Materials Properties.* Graduate Texts in Physics Series, Springer Customer Service Center Gmbh, 2016.

[5] D. Bimberg, N. Kirstaedter, N. N. Ledentsov, Z. I. Alferov, P. S. Kop'ev, and V. M. Ustinov, "Ingaas-gaas quantum-dot lasers," *IEEE Journal of Selected Topics in Quantum Electronics*, vol. 3, pp. 196–205, April 1997.

[6] N. N. Ledentsov, A. R. Kovsh, A. E. Zhukov, N. A. Maleev, S. S. Mikhrin, A. P. Vasil'ev, E. S. Semenova, M. V. Maximov, Y. M. Shernyakov, N. V. Kryzhanovskaya, V. M. Ustinov, and D. Bimberg, "High performance quantum dot lasers on gaas substrates operating in 1.5 /spl mu/m range," *Electronics Letters*, vol. 39, pp. 1126–1128, July 2003.

[7] F. Heinrichsdorff, M.-H. Mao, N. Kirstaedter, A. Krost, D. Bimberg, A. O. Kosogov, and P. Werner, "Room-temperature continuous-wave lasing from

stacked inas/gaas quantum dots grown by metalorganic chemical vapor deposition," *Applied Physics Letters*, vol. 71, no. 1, pp. 22–24, 1997.

[8] J. P. Dowling and G. J. Milburn, "Quantum technology: the second quantum revolution," *Philosophical Transactions of the Royal Society of London A: Mathematical, Physical and Engineering Sciences*, vol. 361, no. 1809, pp. 1655–1674, 2003.

[9] D. Loss and D. P. DiVincenzo, "Quantum computation with quantum dots," *Phys. Rev. A*, vol. 57, pp. 120–126, Jan 1998.

[10] A. Imamoğlu, D. D. Awschalom, G. Burkard, D. P. DiVincenzo, D. Loss, M. Sherwin, and A. Small, "Quantum information processing using quantum dot spins and cavity qed," *Phys. Rev. Lett.*, vol. 83, pp. 4204–4207, Nov 1999.

[11] E. Biolatti, R. C. Iotti, P. Zanardi, and F. Rossi, "Quantum information processing with semiconductor macroatoms," *Phys. Rev. Lett.*, vol. 85, pp. 5647–5650, Dec 2000.

[12] M. Bayer, P. Hawrylak, K. Hinzer, S. Fafard, M. Korkusinski, Z. R. Wasilewski, O. Stern, and A. Forchel, "Coupling and entangling of quantum states in quantum dot molecules," *Science*, vol. 291, no. 5503, pp. 451–453, 2001.

[13] C. Kloeffel and D. Loss, "Prospects for spin-based quantum computing in quantum dots," *Annual Review of Condensed Matter Physics*, vol. 4, no. 1, pp. 51–81, 2013.

[14] T. Ladd, "Quantum dots tuned for entanglement," *Physics*, vol. 5, Jan 2012.

[15] P. Barthelemy and L. M. K. Vandersypen, "Quantum dot systems: a versatile platform for quantum simulations," *Annalen der Physik*, vol. 525, no. 10-11, pp. 808–826.

[16] M. Kroner, K. M. Weiss, B. Biedermann, S. Seidl, S. Manus, A. W. Holleitner, A. Badolato, P. M. Petroff, B. D. Gerardot, R. J. Warburton, and K. Karrai, "Optical detection of single-electron spin resonance in a quantum dot," *Phys. Rev. Lett.*, vol. 100, p. 156803, Apr 2008.

[17] A. Schliwa, M. Winkelnkemper, and D. Bimberg, "Few-particle energies versus geometry and composition of in$_x$ga$_{1-x}$As/GaAs self-organized quantum dots," *Phys. Rev. B*, vol. 79, p. 075443, Feb 2009.

[18] P. Klenovský, P. Steindl, J. Aberl, E. Zallo, R. Trotta, A. Rastelli, and T. Fromherz, "Effect of second-order piezoelectricity on the excitonic structure of stress-tuned in(ga)as/gaas quantum dots," *Phys. Rev. B*, vol. 97, p. 245314, Jun 2018.

[19] J. C. Loredo, N. A. Zakaria, N. Somaschi, C. Anton, L. de Santis, V. Giesz, T. Grange, M. A. Broome, O. Gazzano, G. Coppola, I. Sagnes, A. Lemaitre, A. Auffeves, P. Senellart, M. P. Almeida, and A. G. White, "Scalable performance in solid-state single-photon sources," *Optica*, vol. 3, pp. 433–440, Apr 2016.

[20] N. Somaschi, V. Giesz, L. De Santis, J. C. Loredo, M. P. Almeida, G. Hornecker, S. L. Portalupi, T. Grange, C. Antón, J. Demory, C. Gómez, I. Sagnes, N. D. Lanzillotti-Kimura, A. Lemaítre, A. Auffeves, A. G. White, L. Lanco, and P. Senellart, "Near-optimal single-photon sources in the solid state," *Nature Photonics*, vol. 10, pp. 340 EP –, Mar 2016. Article.

[21] X. Ding, Y. He, Z.-C. Duan, N. Gregersen, M.-C. Chen, S. Unsleber, S. Maier, C. Schneider, M. Kamp, S. Höfling, C.-Y. Lu, and J.-W. Pan, "On-demand single photons with high extraction efficiency and near-unity indistinguishability from a resonantly driven quantum dot in a micropillar," *Phys. Rev. Lett.*, vol. 116, p. 020401, Jan 2016.

[22] G. P. Agrawal, *Fiber-optic communication systems.* Wiley-Blackwell, 2011.

[23] B. Höfer, F. Olbrich, J. Kettler, M. Paul, J. Höschele, M. Jetter, S. L. Portalupi, F. Ding, P. Michler, and O. G. Schmidt, "Tuning emission energy and fine structure splitting in quantum dots emitting in the telecom O-band," *ArXiv e-prints*, feb 2018.

[24] M. Paul, F. Olbrich, J. Höschele, S. Schreier, J. Kettler, S. L. Portalupi, M. Jetter, and P. Michler, "Single-photon emission at 1.55 μm from movpe-grown inas quantum dots on ingaas/gaas metamorphic buffers," *Applied Physics Letters*, vol. 111, no. 3, p. 033102, 2017.

[25] F. Olbrich, J. Höschele, M. Müller, J. Kettler, S. Luca Portalupi, M. Paul, M. Jetter, and P. Michler, "Polarization-entangled photons from an ingaas-based quantum dot emitting in the telecom c-band," *Applied Physics Letters*, vol. 111, no. 13, p. 133106, 2017.

[26] M. Müller, S. Bounouar, K. D. Jöns, M. Glässl, and P. Michler, "On-demand generation of indistinguishable polarization-entangled photon pairs," *Nature Photonics*, vol. 8, pp. 224 EP –, Feb 2014.

[27] R. Takahashi, K. Kono, S. Tarucha, and K. Ono, "Voltage-selective bidirectional polarization and coherent rotation of nuclear spins in quantum dots," *Phys. Rev. Lett.*, vol. 107, p. 026602, Jul 2011.

[28] R. Stockill, C. Le Gall, C. Matthiesen, L. Huthmacher, E. Clarke, M. Hugues, and M. Atatüre, "Quantum dot spin coherence governed by a strained nuclear environment," *Nat Commun*, vol. 7, p. 12745, Sep 2016. 27615704[pmid].

[29] J. H. Prechtel, A. V. Kuhlmann, J. Houel, A. Ludwig, S. R. Valentin, A. D. Wieck, and R. J. Warburton, "Decoupling a hole spin qubit from the nuclear spins," *Nature Materials*, vol. 15, pp. 981 EP –, Jul 2016. Article.

[30] L. Huthmacher, R. Stockill, E. Clarke, M. Hugues, C. Le Gall, and M. Atatüre, "Coherence of a dynamically decoupled quantum-dot hole spin," *Phys. Rev. B*, vol. 97, p. 241413, Jun 2018.

[31] S. C. Lee, A. Stintz, and S. R. J. Brueck, "Nanoscale limited area growth of inas islands on gaas(001) by molecular beam epitaxy," *Journal of Applied Physics*, vol. 91, no. 5, pp. 3282–3288, 2002.

[32] Y. Nagamune, M. Nishioka, S. Tsukamoto, and Y. Arakawa, "Gaas quantum dots with lateral dimension of 25 nm fabricated by selective metalorganic

chemical vapor deposition growth," *Applied Physics Letters*, vol. 64, no. 19, pp. 2495–2497, 1994.

[33] I. Stranski and L. v. Krastanow, "Sitzungsberichte d. akad. d. wissenschaften in wien, abt," *IIb*, vol. 146, p. 797, 1937.

[34] M. Cusack, P. Briddon, and M. a. Jaros, "Electronic structure of inas/gaas self-assembled quantum dots," *Physical Review B*, vol. 54, no. 4, p. R2300, 1996.

[35] I. Kegel, T. Metzger, A. Lorke, J. Peisl, J. Stangl, G. Bauer, J. Garcia, and P. Petroff, "Nanometer-scale resolution of strain and interdiffusion in self-assembled inas / gaas quantum dots," *Physical review letters*, vol. 85, pp. 1694–7, 09 2000.

[36] B. D. Min, Y. Kim, E. K. Kim, S.-K. Min, and M. J. Park, "Suppression of ostwald ripening in $in_{0.5}ga_{0.5}As$ quantum dots on a vicinal (100) substrate," *Phys. Rev. B*, vol. 57, pp. 11879–11882, May 1998.

[37] L.-W. Wang, A. Franceschetti, and A. Zunger, "Million-atom pseudopotential calculation of γ- X mixing in GaAs/AlAs superlattices and quantum dots," *Phys. Rev. Lett.*, vol. 78, pp. 2819–2822, Apr 1997.

[38] L.-W. Wang and A. Zunger, "Linear combination of bulk bands method for large-scale electronic structure calculations on strained nanostructures," *Phys. Rev. B*, vol. 59, pp. 15806–15818, Jun 1999.

[39] A. Zunger, "Pseudopotential theory of semiconductor quantum dots," *Phys. Stat. Sol. (B)*, vol. 224, no. 3, pp. 727–734, 2001.

[40] M. S. Hybertsen and S. G. Louie, "Spin-orbit splitting in semiconductors and insulators from the ab initio pseudopotential," *Phys. Rev. B*, vol. 34, pp. 2920–2922, Aug 1986.

[41] A. J. Williamson, L. W. Wang, and A. Zunger, "Theoretical interpretation of the experimental electronic structure of lens-shaped self-assembled inas/gaas quantum dots," *Phys. Rev. B*, vol. 62, pp. 12963–12977, Nov 2000.

[42] G. Deng and L. W. Cahill, "An adaptive gaussian filter for noise reduction and edge detection," in *1993 IEEE Conference Record Nuclear Science Symposium and Medical Imaging Conference*, vol. 3, pp. 1615–1619, Oct 1993.

[43] P. K. Kythe, *Greens functions and linear differential equations: theory, applications and computation.* Chapman & Hall/CRC, 2011.

[44] J. J. Sakurai, *Modern Quantum Mechanics.* Cambridge University Press, 2017.

[45] A. J. Williamson and A. Zunger, "Pseudopotential study of electron-hole excitations in colloidal free-standing inas quantum dots," *Physical Review B*, vol. 61, no. 3, p. 1978–1991, 2000.

[46] V. I. Lebedev and D. N. Laikov, "A quadrature formula for the sphere of the 131st algebraic order of accuracy," *Doklady Mathematics*, vol. 59, pp. 477–481.

[47] E. Borovitsjaya and M. Shur, *Quantum dots.* World scientific, 2003.

[48] U. Keleş, *Silicon nanowire-based complex structures : A Large-scale atomistic electronic structure and ballistic transport.* PhD thesis, Aug 2016.